Triple oxygen isotope distribution in modern mammal teeth and potential geologic applications

Sophie Lehmann[1], Naomi Levin[2], Benjamin Passey[2], Huanting Hu[3], Thure Cerling[4], Joshua Miller[5], Laura Arppe[6], Emily Beverly[7], Kathryn Hoppe[8], Julie Luyt[9], and Judith Sealy[9]

[1]Department of Geology and Environmental Science, University of Pittsburgh
[2]Department of Earth and Environmental Sciences, University of Michigan
[3]School of Oceanography, Shanghai Jiao Tong University
[4]Department of Biology and Department of Geology and Geophysics, University of Utah
[5]Department of Geology, University of Cincinnati
[6]Finnish Museum of Natural History, University of Helsinki
[7]Department of Earth and Atmospheric Sciences, University of Houston
[8]Green River College and Burke Museum, University of Washington
[9]Department of Archaeology, University of Cape Town

November 24, 2022

Abstract

Reconstructing water availability in terrestrial ecosystems is key to understanding past climate and landscapes, but there are few proxies for aridity that are available for use at terrestrial sites across the Cenozoic. The isotopic composition of tooth enamel is widely used as paleoenvironmental indicator and recent work suggests the potential for using the triple oxygen isotopic composition of mammalian tooth enamel ([?]'17Oenamel) as an indicator of aridity. However, the extent to which [?]'17Oenamel values vary across environments is unknown and there is no framework for evaluating past aridity using [?]'17Oenamel data. Here we present [?]'17Oenamel and δ18Oenamel values from 50 extant mammalian herbivores that vary in physiology, behavior, diet, and water-use strategy. Teeth are from sites in Africa, Europe, and North America and represent a range of environments (humid to arid) and latitudes (34S to 69N), where mean annual δ18O values of meteoric water range from -26.0to 2.2(-283 to -137 per meg, where 1 per meg = 0.001in [?]'17Oenamel values increases with aridity, forming a wedged-shape pattern in a plot of aridity index vs. [?]'17Oenamel that persists regardless of region. In contrast, the plot of aridity index vs. δ18Oenamel for these same samples does not yield a distinct pattern. We use these new [?]'17Oenamel data from extant teeth to provide guidelines for using [?]'17Oenamel data from fossil teeth to assess and classify the aridity of past environments. [?]'17Oenamel values from the fossil record have the potential to be a widely used proxy for aridity without the limitations inherent to approaches that use δ18Oenamel values alone. In addition, the data presented here have implications for how [?]'17Oenamel values of large mammalian herbivores can be used in evaluations of diagenesis and past pCO2.

Hosted file

`essoar.10506275.1.docx` available at https://authorea.com/users/551081/articles/604220-triple-oxygen-isotope-distribution-in-modern-mammal-teeth-and-potential-geologic-applications

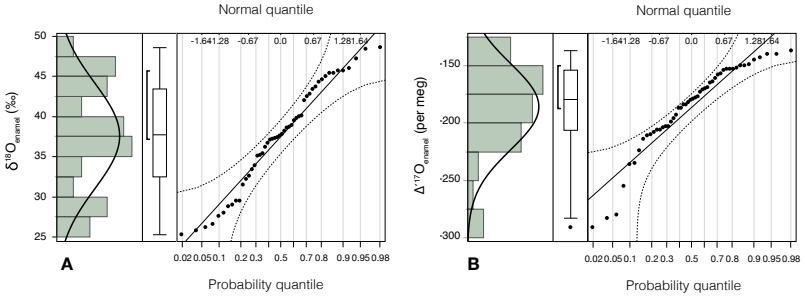

Triple oxygen isotope distribution in modern mammal teeth and potential geologic applications

Authors

Sophie B. Lehmann[1], Naomi E. Levin[2], Benjamin H. Passey[2], Huanting Hu[3], Thure E. Cerling[4, 5], Joshua H. Miller[6], Laura Arppe[7], Emily J. Beverly[8], Kathryn A. Hoppe[9,10], Julie Luyt[11], Judith Sealy[11]

Affiliations

[1] Department of Geology and Environmental Science, University of Pittsburgh, Pittsburgh, PA, 15260; sophie.b.lehmann@gmail.com

[2] Department of Earth and Environmental Sciences, University of Michigan, 1100 North University Avenue, Ann Arbor, MI, 48103, USA; passey@umich.edu, nelevin@umich.edu

[3] School of Oceanography, Shanghai Jiao Tong University; huanting.hu@sjtu.edu.cn

[4] Department of Biology and [5]Department of Geology and Geophysics, University of Utah, Salt Lake City, UT 84112; thure.cerling@utah.edu

[6] Department of Geology, University of Cincinnati, Cincinnati, Ohio, 45221, USA; josh.miller@uc.edu

[7] Finnish Museum of Natural History, University of Helsinki, Helsinki, Finland; laura.arppe@helsinki.fi

[8] Department of Earth and Atmospheric Sciences, University of Houston, Houston, Texas 77204; ejbeverly@uh.edu

[9] Green River College and [10] Burke Museum, University of Washington; khoppe@greenriver.edu

[11] Department of Archaeology, University of Cape Town, South Africa; Julie.luyt@uct.ac.za, Judith.Sealy@uct.ac.za

Highlights

- We present $\Delta'^{17}O$ data from 50 teeth from 7 mammal families and 3 continents.
- $\Delta'^{17}O_{enamel}$ values of animals from a single environment span up to 146 per meg.
- $\Delta'^{17}O_{enamel}$ is insensitive to geographic variables affecting $\delta^{18}O_{meteoric\ water}$.
- $\Delta'^{17}O_{enamel}$ from arid sites are lower and more variable than from mesic sites.
- $\Delta'^{17}O_{enamel}$ can be used as an indicator of aridity.

Keywords

Aridity, mammalian teeth, paleoclimate, environment, stable isotopes, triple oxygen isotopes

Abstract

Reconstructing water availability in terrestrial ecosystems is key to understanding past climate and landscapes, but there are few proxies for aridity that are available for use at terrestrial sites across the Cenozoic. The isotopic composition of tooth enamel is widely used as paleoenvironmental indicator and recent work suggests the potential for using the triple oxygen isotopic composition of mammalian tooth enamel ($\Delta'^{17}O_{enamel}$) as an indicator of aridity. However, the extent to which $\Delta'^{17}O_{enamel}$ values vary across environments is unknown and there is no framework for evaluating past aridity using $\Delta'^{17}O_{enamel}$ data. Here we present $\Delta'^{17}O_{enamel}$ and $\delta^{18}O_{enamel}$ values from 50 extant mammalian herbivores that vary in physiology, behavior, diet, and water-use strategy. Teeth are from sites in Africa, Europe, and North America and represent a range of environments (humid to arid) and latitudes (34°S to 69°N), where mean annual $\delta^{18}O$ values of meteoric water range from -26.0‰ to 2.2‰ (VSMOW). $\Delta'^{17}O_{enamel}$ values from these sites span 154 per meg (-291 to -137 per meg, where 1 per meg = 0.001‰). The observed variation in $\Delta'^{17}O_{enamel}$ values increases with aridity, forming a wedged-shape pattern in a plot of aridity index vs. $\Delta'^{17}O_{enamel}$ that persists regardless of region. In contrast, the plot of aridity index vs. $\delta^{18}O_{enamel}$ for these same samples does not yield a distinct pattern. We use these new $\Delta'^{17}O_{enamel}$ data from extant teeth to provide guidelines for using $\Delta'^{17}O_{enamel}$ data from fossil teeth to assess and classify the aridity of past environments. $\Delta'^{17}O_{enamel}$ values from the fossil record have the potential to be a widely used proxy for aridity without the limitations inherent to approaches that use $\delta^{18}O_{enamel}$ values alone. In addition, the data presented here have implications for how $\Delta'^{17}O_{enamel}$ values of large mammalian herbivores can be used in evaluations of diagenesis and past pCO_2.

1. Introduction and Background

1.1. Traditional use of oxygen isotopes in tooth enamel as climatic and environmental proxies

The distribution of oxygen isotopes in marine and terrestrial carbonates (e.g., foraminifera tests, soil and lake carbonates, tooth enamel) has long been used to reconstruct climate, environment, and surface processes (e.g., Zachos et al., 2001; Rowley and Currie, 2006; Blumenthal et al., 2017). Oxygen isotope values ($\delta^{18}O$) of carbonate vary with environmental conditions and geography because they reflect the $\delta^{18}O$ value of the waters from which they form. The $\delta^{18}O$ value of meteoric-derived waters (e.g., rain, rivers, lakes, groundwater) varies relative to climate and hydrology because it is sensitive to both equilibrium (e.g., temperature changes, Rayleigh distillation) and kinetic (e.g., evaporation) oxygen isotope fractionation effects (e.g., Rozanski et al., 1993). However, the influence of these isotope effects on the $\delta^{18}O$ values can be difficult to tease apart.

Fossil mammalian teeth are found globally, span the Cenozoic, and are used as environmental indicators. The $\delta^{18}O$ value of tooth enamel ($\delta^{18}O_{enamel}$) is an alluring climate proxy because it often tracks $\delta^{18}O$ values of meteoric water, but this relationship is sensitive to an animal's diet, physiology, and water-use strategy (Kohn, 1996). An individual's $\delta^{18}O_{enamel}$ values and their use as paleoclimate indicators are impacted by a variety of factors, including the animal's intake of atmospheric O_2 (accounting for 5–40% of oxygen in body water), its water-use efficiency, and the degree of evaporation of ingested waters (plant waters, surface waters) relative to local precipitation. Because $\delta^{18}O_{enamel}$ values have a variety of influences, they have been used to track a range of processes. Some studies estimate changes in paleotemperature from $\delta^{18}O_{enamel}$ values, relying on the assumption that $\delta^{18}O_{enamel}$ values track the $\delta^{18}O$ value of

84 meteoric water, which vary with temperature at mid to high latitudes (e.g., Fricke et al., 1995).
85 However, this approach does not account for variability in $\delta^{18}O$ values of ingested waters within
86 an ecosystem, where leaf and drinking waters can be several per mil (‰) higher than
87 unevaporated meteoric water. Other approaches leverage these differences in evaporation and
88 use $\delta^{18}O_{enamel}$ values from animals with different diets and behaviors to separate the influence of
89 evaporative enrichment on $\delta^{18}O_{enamel}$ values and then estimate past aridity (Levin et al., 2006;
90 Blumenthal et al., 2017). This "aridity index" approach categorizes animals by their water-use
91 strategy where evaporation-insensitive (EI) taxa, like Hippopotamidae, ingest a relatively large
92 amount of drinking water, in contrast to evaporation-sensitive (ES) taxa, like Giraffidae, which
93 require less drinking water. The offset between $\delta^{18}O_{enamel}$ values of ES and EI taxa increases with
94 aridity. While the $\delta^{18}O_{enamel}$ aridity indicator is powerful, it is tuned to Quaternary mammal
95 assemblages in eastern Africa (Blumenthal et al., 2017) and not easily transferrable to older
96 periods or different regions without making assumptions about animal behavior and
97 physiology.
98
99 *1.2. Triple oxygen isotopic composition of waters and carbonates*
100 Triple oxygen isotope (^{18}O-^{17}O-^{16}O) distributions in water and near-surface minerals (e.g.,
101 carbonate, gypsum) have potential as indicators of aridity because they are sensitive to kinetic
102 and equilibrium isotope effects and can track the influence of evaporation (Barkan and Luz,
103 2005; 2007; Li et al., 2017; Surma et al., 2018; Passey and Levin, 2021).
104 The majority of processes involving oxygen isotopic fractionation on Earth are mass
105 dependent and governed by the power law relationship $^{17}\alpha_{a\text{-}b} = {}^{18}\alpha_{a\text{-}b}{}^{\theta}$, where the isotopic

fractionation between two materials or phases, a and b, is defined as $\alpha_{a\text{-}b} = R_a/R_b$ and R represents the ratio of the heavy to light isotope ($^{18}O/^{16}O$, $^{17}O/^{16}O$) (Matsuhisa et al., 1978; Young et al., 2002). Although these relationships have been well known for the past 40 years, differences in the exponent θ were considered too small to detect with most analytical approaches and there was little motivation for analyzing $\delta^{17}O$ as it provided the same information as $\delta^{18}O$. However, efforts to increase analytical precision yield empirical and experimental studies that showed measurable distinctions in θ between kinetic and equilibrium fractionation processes. These distinctions are particularly evident in the hydrosphere where θ is 0.529 for equilibrium exchange between water liquid and vapor, but 0.5185 for the diffusion of water through air that occurs during evaporation (Young et al., 2002; Barkan and Luz, 2005; 2007).

These θ values are equivalent to the slope on a $\delta'^{18}O$ - $\delta'^{17}O$ plot, where $\delta^xO = (R_{sample}/R_{standard} - 1)*1000$ and $\delta'^xO = \ln(R_{sample}/R_{standard})$, and x = 17 or 18. Given the small distinctions in slope that differentiate equilibrium and kinetic fractionation (0.529 vs. 0.5185), we use $\Delta'^{17}O$ to visualize and discuss triple oxygen isotope variation, where λ represents the slope in the $\delta'^{18}O$ - $\delta'^{17}O$ plot and is the mathematical equivalent to θ (Miller, 2002). Larger deviations and more negative $\Delta'^{17}O$ values reflect a greater influence of evaporation (Figs. 1–2). In this study, we use λ instead of θ to characterize ^{18}O-^{17}O-^{16}O distributions because it represents the relationship between the fractionation of $^{18}O/^{16}O$ and $^{17}O/^{16}O$ values during a combination of processes, whereas θ characterizes this relationship for a single process (Barkan and Luz, 2005; 2007).

Meteoric-derived waters like rain, river, lake and ground waters have $\Delta'^{17}O$ values that range from -56 to +60 per meg (Landais et al., 2006, 2010; Barkan and Luz, 2011; Surma et al.,

2015, 2018; Li et al., 2017; Passey and Ji, 2019; Uechi and Uemura, 2019). However, exceptions include evaporated ponds in the Atacama Desert and in the Sistan Oasis that yield much lower $\Delta'^{17}O$ values (~-70 per meg and -167 per meg, respectively) (Surma et al., 2015; 2018; Herwartz et al., 2017). Plant water $\Delta'^{17}O$ values are typically more sensitive to evaporation than meteoric-derived waters, ranging from -271 to +35 per meg (Fig. 1).

Similar to $\delta^{18}O_{enamel}$ values, $\Delta'^{17}O$ values of mammalian tooth enamel ($\Delta'^{17}O_{enamel}$) are influenced by the isotopic composition of food, drinking water, and atmospheric O_2 (Pack et al., 2013). The $\Delta'^{17}O$ value of O_2 is distinct and considerably lower than water, with a value of -432±15 per meg (1σ) recommended by Pack (2021) based on a compilation of data from the recent literature (Fig. 1). Relative humidity has a particularly strong influence on body water $\Delta'^{17}O$ values of mammalian herbivores because it reflects the degree of evaporation of ingested water (Passey and Levin, 2021; Hu et al., *in revision*).

Given the strong influence of evaporation on the oxygen isotopes of body water, we expect $\Delta'^{17}O_{enamel}$ values to vary with environment (Fig. 2B) such that they can be used as indicators of past aridity. Models of isotopic fractionation in body water suggest that animals who ingest the majority of their water from plants should have more negative $\Delta'^{17}O_{enamel}$ values than animals that drink water regularly due to evaporative enrichment of plant/leaf water relative to surface waters (Passey and Levin, 2021; Hu et al., *in revision*; Fig. 2C). Given this, we predict that $\Delta'^{17}O_{enamel}$ values will exhibit more variance in arid environments regardless of taxa and meteorological/climatic features that vary according to geographic location of a site.

Here we present the $\Delta'^{17}O_{enamel}$ values of teeth from 50 extant herbivores from seven mammalian families and three continents to demonstrate variation in $\Delta'^{17}O_{enamel}$ values across

different environments. We then outline approaches to using $\Delta'^{17}O_{enamel}$ records to reconstruct past aridity, in addition to its use in assessing post-depositional alteration of enamel oxygen isotopes and as a pCO_2 indicator.

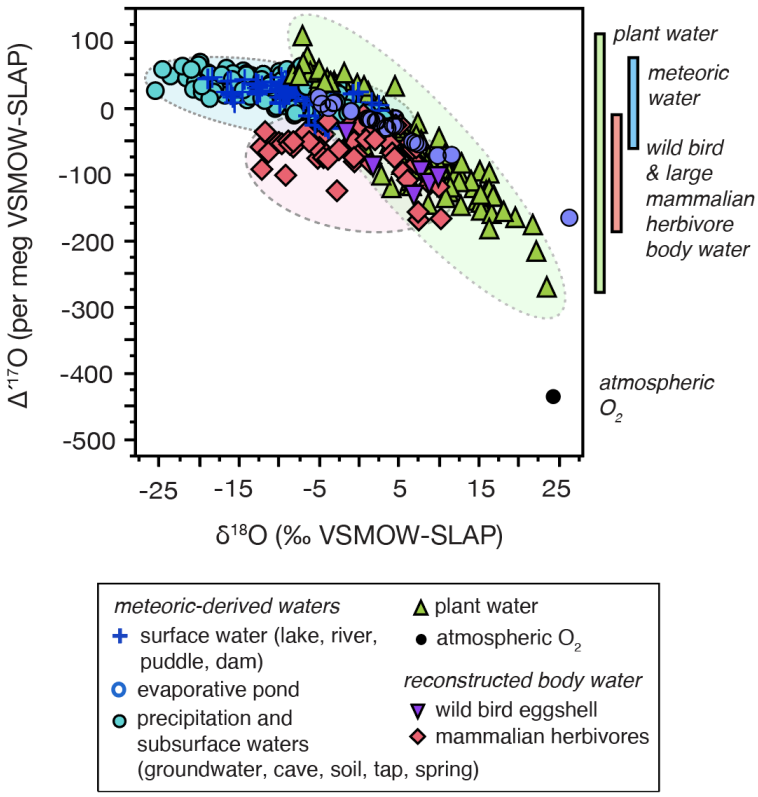

Figure 1: $\Delta'^{17}O$ and $\delta^{18}O$ values of reconstructed body water for extant mammalian herbivores and birds and their primary input sources of oxygen: ingested plant water and drinking water, and inhaled atmospheric O_2. Body water $\Delta^{17}O$ values are calculated from teeth and eggshells (BW $\Delta'^{17}O = \Delta'^{17}O_{enamel\ or\ eggshell} - (\lambda - 0.528) * (1000 * \ln(^{18}\alpha))$, where $\lambda = 0.5245$, $^{18}\alpha = 1.0332$ for teeth, and $^{18}\alpha = 1.0332$ for eggshells as in Passey et al. (2014)). Meteoric-derived waters are

separated into the categories precipitation and subsurface waters, surface waters, and evaporative ponds. Vertical bars on right show the range of $\Delta'^{17}O$ values for sources of oxygen for mammals and their reconstructed body waters. Data are from Landais et al. (2006, 2010), Luz and Barkan (2010), Barkan and Luz (2011), Passey et al. (2014), Li et al. (2017), Surma et al. (2015; 2018), Herwartz et al. (2017), Passey and Ji (2019), Uechi and Uemura (2019), Whiteman et al. (2019), Pack et al. (2021); Hu et al. (*in revision*), and this study.

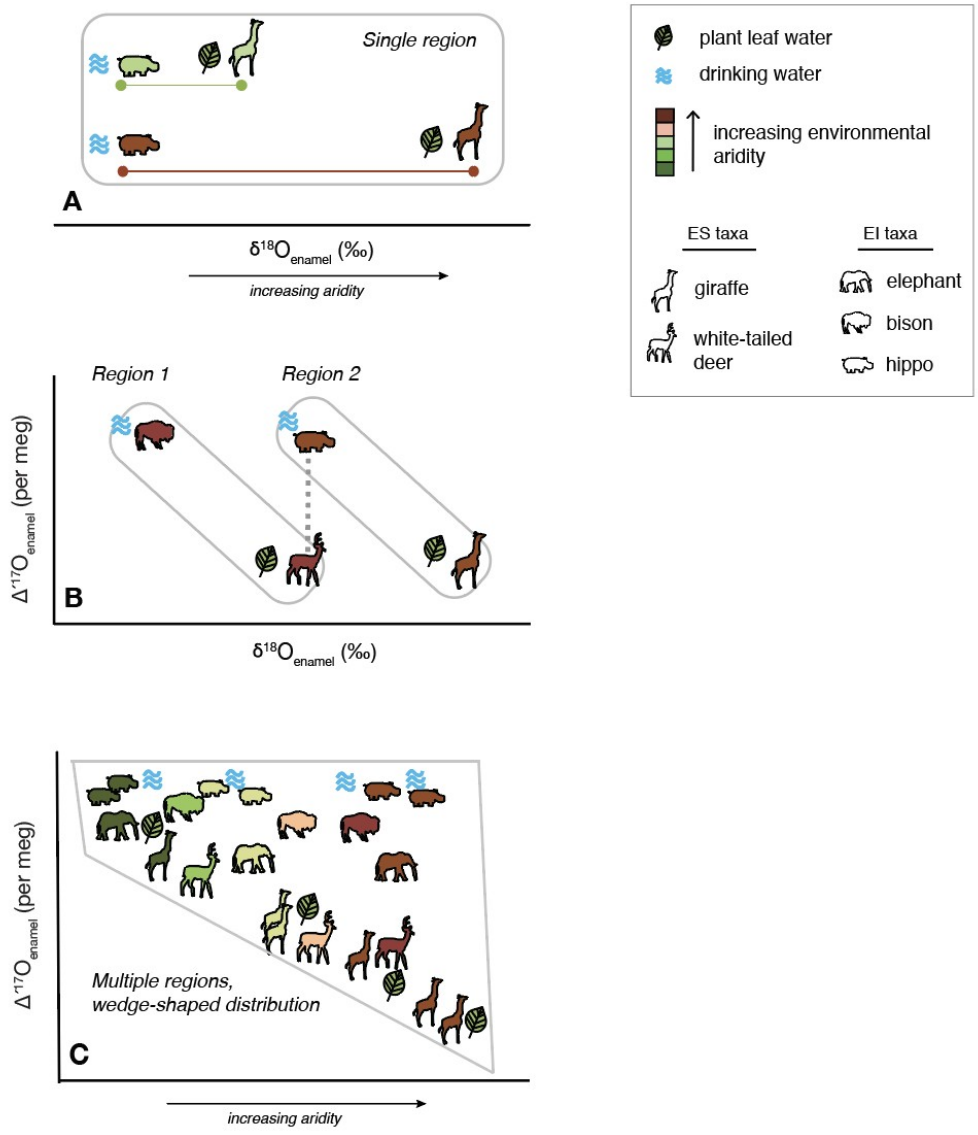

Figure 2: Schematics outlining the variation of $\delta^{18}O_{enamel}$ and $\Delta'^{17}O_{enamel}$ values with aridity. A) The $\delta^{18}O_{enamel}$ value of evaporative sensitive (ES) and evaporative insensitive (EI) taxa from two environments within a single region where the $\delta^{18}O$ value of drinking water is constant. B) The $\delta^{18}O_{enamel}$ and $\Delta'^{17}O_{enamel}$ values of ES and EI taxa from environments with the same degree of aridity but from different regions, where $\delta^{18}O$ values of drinking water vary. Dashed gray line indicates how $\delta^{18}O_{enamel}$ values cannot distinguish a circumstance where aridity and input $\delta^{18}O$ values vary, whereas this distinction can be made with $\Delta'^{17}O_{enamel}$ values. C) Variation in $\Delta'^{17}O_{enamel}$ values vs. aridity for various locations and taxa spanning a range of behaviors and water-use strategies, showing a predicted wedge-shaped pattern.

2. Materials and Methods

2.1. Site and sample selection

We designed our sample selection to evaluate the triple oxygen isotope distribution of teeth from large (> 6 kg), extant mammalian herbivores that represented a range of water-use strategies and behaviors, continents, latitudes, and climates (Supplementary Table 1). We analyzed teeth from Hippopotamidae (*n*=4), Elephantidae (*n*=9), Bovidae (*n*=9), Castoridae (*n*=2), Cervidae (*n*=15) and Giraffidae (*n*=6). These data were combined with already published data from a Hippopotamidae, Bovidae, and Rhinocerotidae from Passey et al. (2014) and a Cervidae and Bovidae from Hu et al. (*in revision*). Teeth were collected over the past five decades and many samples have been used in previous studies (Supplementary Table 2). Specimens from Europe are from the Finnish Museum of National History.

192

193 *2.2. Climate and aridity of sites*

194 The geographic and climatic parameters for sites for which we report tooth enamel
195 triple oxygen isotope data are listed in Table 1. We extracted mean annual temperature (MAT),
196 precipitation (MAP), potential evapotranspiration (PET), percent relative humidity (rh), and
197 Aridity Index (AI, where AI=MAP/PET) estimates for each location using the WorldClim Global
198 Climate Data raster 1.4, or WorldCim1.4 (Hijmans et al., 2005; Trabucco and Zomer, 2009). We
199 assigned corresponding UNESCO climate classifications to sites using AI data: arid, semi-arid,
200 subhumid, and humid (UNESCO, 1979). The $\delta^{18}O$ values of mean annual meteoric water (‰
201 VSMOW) were calculated using waterisotopes.org (Bowen and Revenaugh, 2003).

202

203 *2.3. Sample preparation and analysis*

204 Enamel was removed along the growth axis of the tooth, cleared of dentine and dirt,
205 powdered, and homogenized. Powder was treated with 3% H_2O_2 to remove organic material,
206 bathed in buffered acetic acid (0.1 *M*) to remove secondary carbonate, and dried at 60°C. Analysis
207 of triple oxygen isotopes of enamel followed the procedure outlined in Passey et al. (2014). Briefly,
208 enamel powder (140 – 200 mg per analysis) was placed in silver capsules and reacted in a common
209 bath of 100% phosphoric acid under vacuum at 90°C to extract CO_2. CO_2 was then reduced to H_2O
210 (Fe powder catalyst, 560°C, 20 minutes), which was then fluorinated by passing through cobalt
211 trifluoride at 370°C. The resultant O_2 was then analyzed by duel inlet isotope ratio mass
212 spectroscopy on a Thermo Scientific MAT 253 at Johns Hopkins University. Samples were analyzed
213 in duplicate. We evaluated the stability of isotope measurements of external carbonate standards,

both international (NBS18 and NBS19) and in-house (102-GC-AZ01) carbonates, and an inhouse CO_2 gas standard (Tank#2 CO_2). Water standards SLAP2 and VSMOW2 were directly injected into the cobalt trifluoride reactor to produce O_2 gas. The pooled standard deviation (1σ) for the external carbonate and CO_2 standards was 0.9‰ for $\delta^{18}O$ and 10 per meg for $\Delta'^{17}O$ over the time period when the samples were analyzed.

Carbonate oxygen isotope data were normalized to VSMOW2 ($\delta^{18}O$=0‰ and $\delta^{17}O$=0 per meg) and scaled to SLAP2 ($\delta^{18}O$=-55.5‰) using the reference frame $\Delta'^{17}O_{SLAP2}$=0 per meg, where $\delta^{17}O_{SLAP2}$=-29.6986‰ when $\delta^{18}O_{SLAP2}$=-55.5‰ and λ=0.528 (Schoenemann et al., 2013). A secondary normalization step was performed for carbonates to correct for offsets between observed and accepted $\delta^{18}O$ values (Passey et al., 2014). Finally, we compared $\Delta'^{17}O$ of international and internal standards analyzed during each session to values reported in Passey et al., 2014 (NBS18=-98 per meg; NBS19=-135 per meg; 102-GC-AZ01=-94 per meg; Tank#2 CO_2=118 per meg). If a significant difference was observed, we applied a correction to all carbonate $\Delta'^{17}O$ data from that session based on the residual from the Passey et al. (2014) $\Delta'^{17}O$ values, averaged for all standards analyzed within that session. Of the six analytical sessions in this study, three required such correction, with magnitudes of -40 per meg (July 2015), -13 per meg (August 2015 session 1), and -31 per meg (August 2015 session 2). We note that Wostbrock et al. (2020) report $\Delta'^{17}O$ values for CO_2 extracted from NBS18 and NBS19 (25℃ reaction) with phosphoric acid of -100 per meg and -155 per meg, respectively (compared to -98 per meg and -135 per meg in Passey et al., 2014). Sharp and Wostbrock (2021) recommend normalizing $\Delta'^{17}O$ data to the values reported in Wostbrock et al. (2020). We fundamentally agree with this recommendation, but refrain here because our samples were reacted using a different phosphoric acid temperature (90℃ instead of

25°C in Wostbrock and Sharp, 2020), and it is yet unknown how triple oxygen isotope acid fractionation scales with temperature of acid digestion. Regardless, all data for standards are reported Supplementary Table 3, which will allow for subsequent renormalization of our dataset when the necessary fractionation factors are determined.

All data from analytical sessions are reported in Supplementary Table 4 (i.e., raw and corrections). Data were evaluated using the statistical analytical software JMP 11 produced by the SAS Institute. The ± symbol indicates one standard deviation from the mean and data are frequently reported as mean ±1σ. Throughout the text, oxygen isotope measurements are described using $\Delta'^{17}O$ and $\delta^{18}O$ notation, δ-values are reported in per mil (‰), and $\Delta'^{17}O$ values are reported in per meg, where 1‰ is 1000 per meg and defined with a reference slope of 0.528.

We used pairwise analyses to evaluate isotopic differences between latitudes, families, and climate categories. However, while our $\delta^{18}O_{enamel}$ data are normally distributed, our $\Delta'^{17}O_{enamel}$ data deviate from normality (Supplementary Fig. 1). Due to these differences, we use parametric ANOVA tests to evaluate $\delta^{18}O_{enamel}$ and nonparametric Wilcoxon and Kruskal-Wallis tests to evaluate $\Delta'^{17}O_{enamel}$. Differences among-group were evaluated using Tukey-Kramer HSD and the Steel-Dwass Method. To test for differences in variance across climate, we used the parametric Bartlett's test and nonparametric Levene's test for $\delta^{18}O_{enamel}$ and $\Delta'^{17}O_{enamel}$, respectively. Within each family, we used linear regression to evaluate the relationship between changes in aridity and associated changes in isotope values. All isotope values from a common family at a single site are first summarized as the median value before evaluating the linear regression to account for non-independence.

3. Results

3.1. Variation by latitude and region

Among all the herbivores, $\Delta'^{17}O_{enamel}$ values range from -291 to -137 per meg (-186±37 per meg) and $\delta^{18}O_{enamel}$ values range from 25.3‰ to 48.6‰ (37.6±6.6‰) (Supplementary Table 1; Fig. 3). $\Delta'^{17}O_{enamel}$ values do not vary with absolute latitude (R^2=0.017, p=0.1965). $\delta^{18}O_{enamel}$ values decrease with increasing absolute latitude (R^2=0.628, p=<0.0001), such that teeth sampled from low latitudes (0 – 24˚, n=24) yield $\delta^{18}O_{enamel}$ values that are significantly different (p>0.0001) than those from mid latitudes (24 – 66˚, n=21) (Fig. 3 A – C). The lack of obvious differences in the $\delta^{18}O_{enamel}$ values from mid and high latitudes may be an artifact of limited samples from high latitudes (> 66˚, n=3).

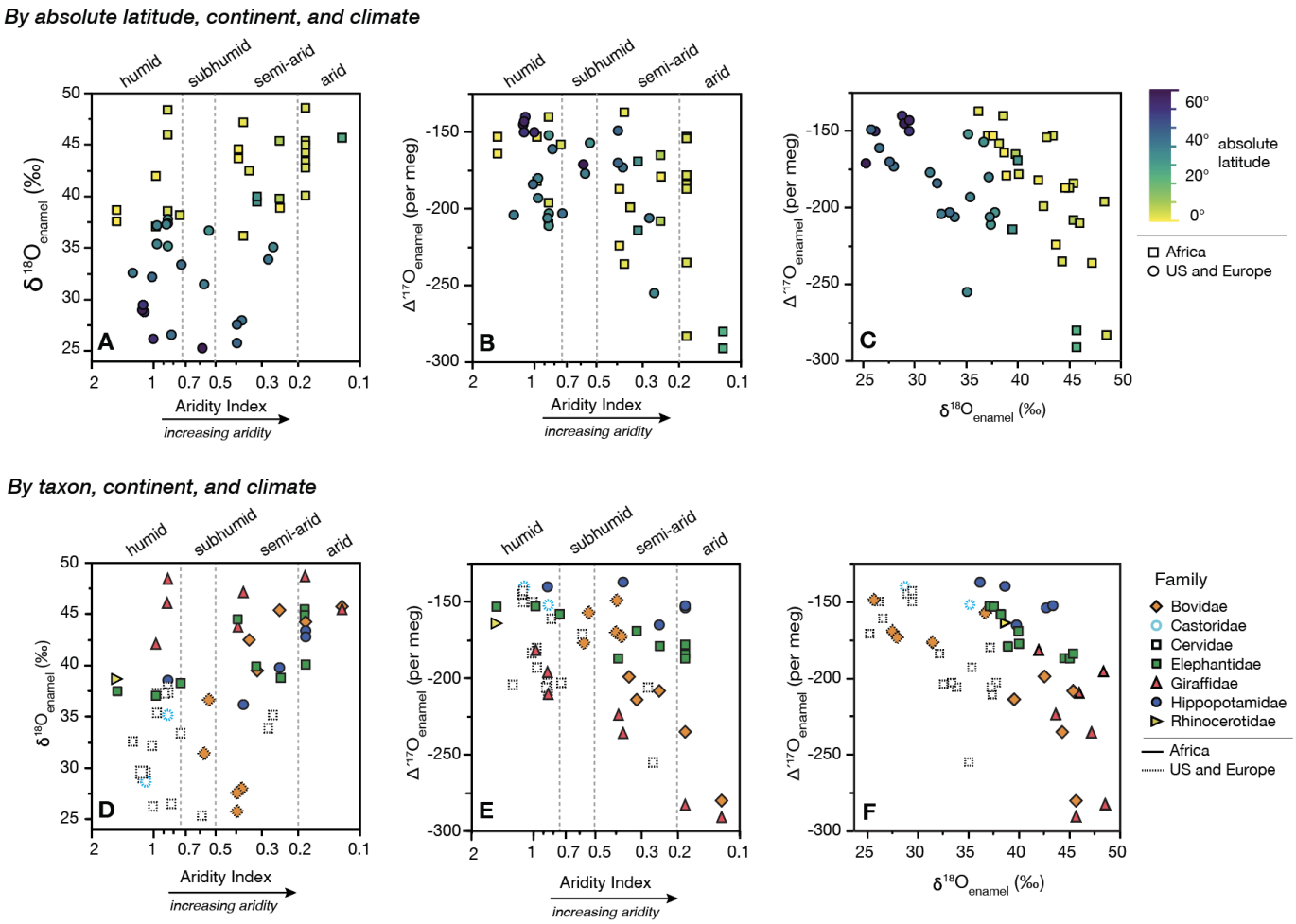

Figure 3: Distribution of $\delta^{18}O_{enamel}$ and $\Delta'^{17}O_{enamel}$ values by latitude, location, taxon, and climate. In plots A – C, the geography of sample site is indicated using a color gradient for absolute latitude and symbols according to region. In plots D – F, taxa are grouped by family. Aridity Index is presented on a log scale and corresponding UNESCO climate categories are separated by vertical dashed lines.

3.2. Variation by aridity

Teeth come from a range of environments where AI values range from 0.12 to 1.52 (Table 1). Environments were placed into UNESCO climate classifications using AI data and characterized as humid (AI > 0.75, *n*=22), subhumid (AI 0.5 – 0.75, *n*=3), semi-arid (AI 0.2 – 0.5, *n*=16), and arid (AI < 0.2, *n*=9) (UNESCO, 1979). They include the arid Turkana and Kgalagadi regions (AI 0.18 and 0.12, respectively), mid latitude semi-arid Utah (AI 0.26), high latitude, cold, subhumid Alaska (AI 0.58), moist highlands in Kenya (AI 1.51), and cool, humid Finland (AI > 1.01).

The distribution of $\Delta'^{17}O_{enamel}$ values form a wedge-shaped pattern when plotted against AI. $\Delta'^{17}O_{enamel}$ values from arid and semi-arid sites (*n*=25, -283 to -137 per meg, -196±43 per meg) have statistically different variance from subhumid and humid sites (*n*=25, -210 to -138 per meg, -170±24 per meg) (df=1, F=7.4179, *p*=0.0090). The $\delta^{18}O_{enamel}$ values from more arid sites (25.5 to 47.5‰, 39.5±6.0‰) are not different from more mesic sites (25.0 to 47.2‰, 34.2±5.7‰) (df=1, F=0.0063, *p*=0.9371).

3.3. Variation by taxon

We observe that herbivore $\Delta'^{17}O_{enamel}$ and $\delta^{18}O_{enamel}$ values vary by taxonomy (Table 2; Supplementary Table 5; Fig. 3 D – F).

In Africa, our sample includes giraffids (*n*=7), bovids (*n*=5), a rhinocerotid (*n*=1), elephantids (*n*=9) and hippopotamids (*n*=5) from South Africa, Kenya, Uganda, and the Democratic Republic of the Congo. The $\Delta'^{17}O_{enamel}$ values of hippopotamids are similar to elephantids (*p*=0.3766) and are significantly higher than those of giraffids (*p*=0.0295). Giraffid and bovid $\Delta'^{17}O_{enamel}$ values are similar (*p*=0.9620) and show large ranges in $\Delta'^{17}O_{enamel}$ (> 100 per

meg). In these groupings, giraffids include samples of giraffe and okapi while the bovids include samples from buffalo, wildebeest, oryx and hartebeest. Giraffid and bovid $\Delta'^{17}O_{enamel}$ values are negatively correlated with AI (bovids, R^2=0.950, p=0.0031; giraffids, R^2=0.860, p=0.0049). In contrast, $\Delta'^{17}O_{enamel}$ values for elephantids and hippopotamids exhibit a narrow range across AI (< 35 per meg) and have R^2=0.467 (p=0.0543) and R^2=0.049 (p=0.3950), respectively. The distribution of $\delta^{18}O_{enamel}$ values of the different taxa mostly overlap with one another. The correlations between $\delta^{18}O_{enamel}$ values and AI are R^2=-1.403 (p=0.5104) for hippopotamids, R^2=0.316 (p=0.1097) for elephantids, R^2=0.360 (p=0.1691) for bovids, and R^2=0.0461 (p=0.3276) for giraffids.

The samples from North America and Europe include teeth from bovids (n=5), castorids (n=2) and cervids (n=16). The $\Delta'^{17}O_{enamel}$ values of castorids and bovids represent a tighter range (-177 to -140 per meg, -160±14 per meg) than that of cervids (-255 to -143 per meg, -185±31 per meg). In comparison, the ranges of cervid and bovid $\delta^{18}O_{enamel}$ are similar across AI (dif mean=2.414550, p=0.507). Castorids from humid environments and their $\delta^{18}O_{enamel}$ values overlap with those of cervids and bovids from humid to semi-arid environments.

Although not visible on Figure 3, where data are grouped by family, it is important to note that three species of cervids were sampled (moose n=3, reindeer/caribou n=3, and white-tailed deer n=10) spanning humid to semi-arid environments. White-tailed deer yield lower $\Delta'^{17}O_{enamel}$ values than that of moose and reindeer/caribou. There is no equivalent distinction in $\delta^{18}O_{enamel}$ values.

4. Discussion

4.1. Variation of $\Delta'^{17}O_{enamel}$ values

4.1.1. Observations

The $\Delta'^{17}O_{enamel}$ values from extant herbivores from Africa, Europe and North America span 146 per meg (-283 to -137 per meg) and can vary by 146 per meg at sites with data from multiple taxa. In comparison, the $\Delta'^{17}O$ values of plant waters span up to 189 per meg in a single environment (Li et al., 2017) and are sensitive to variation in rh between environments (Alexandre et al., 2018), while the $\Delta'^{17}O$ values of meteoric waters across all environments span 85 per meg (Landais et al., 2006; 2010; Luz and Barkan, 2010; Passey et al., 2014; Li et al. 2017; Passey and Ji, 2019).

Aridity seems to be the strongest determinant of $\Delta'^{17}O_{enamel}$ values. We observe a greater variation in $\Delta'^{17}O$ in arid and semi-arid environments, than in humid environments, resulting in a wedge-shaped pattern in a plot of AI vs. $\Delta'^{17}O_{enamel}$ that persists across a range of latitudes and $\delta^{18}O$ values of meteoric water (Fig. 3B). No similar relationship between $\delta^{18}O_{enamel}$ and aridity exists (Fig. 3A). Instead, $\delta^{18}O_{enamel}$ more closely tracks latitude, reflecting the well-known correlation between $\delta^{18}O$ values of meteoric water and latitude (e.g., Dansgaard, 1964).

This wedge-shaped $\Delta'^{17}O_{enamel}$ – aridity relationship occurs when taxa with a range of water-use strategies are sampled. As discussed above, water-use strategy is influenced by diet, physiology, and behavior. An important factor is a taxon's water dependence, which can be characterized by the Water Economy Index (WEI), where WEI=ml H_2O ingested per kJ of metabolic energy (see Nagy and Peterson, 1988). Animals with low WEI values are less dependent on surface waters and can more readily sustain water requirements based on

dietary water (leaf water, root/stem water, metabolic water; Kohn, 1996). Oxygen isotope distributions in animals generally group into two categories, evaporation sensitive (ES) and evaporation insensitive (EI), where $\delta^{18}O_{enamel}$ values of EI taxa (high WEI) do not vary with aridity and $\delta^{18}O_{enamel}$ values of ES taxa (low WEI) increase with aridity (Levin et al., 2006; Blumenthal et al., 2017). We classify taxa as ES or EI using previously published work when possible and otherwise assign a suggested ES or EI classification based on an animal's water and food intake (Table 2).

When $\Delta'^{17}O_{enamel}$ data from the entire dataset are pooled and taxa are grouped by ES and EI classification, $\Delta^{17}O_{enamel}$ values of ES taxa are both lower and more varied than those of EI taxa (Fig. 4A). The distinctions in $\Delta'^{17}O_{enamel}$ values between ES and EI taxa persist across the three continents and the different climate regimes. In contrast, $\delta^{18}O_{enamel}$ values of ES and EI taxa are not distinct, in part because they are strongly influenced by local meteoric water $\delta^{18}O$ values which exert a stronger influence on $\delta^{18}O_{enamel}$ values than animal water-use strategies (Fig. 4B). The clear distinctions in $\Delta'^{17}O_{enamel}$ values between ES and EI taxa show the importance of including samples from taxa with a range of water-use strategies to assess the distribution of $\Delta'^{17}O_{enamel}$ values from any location.

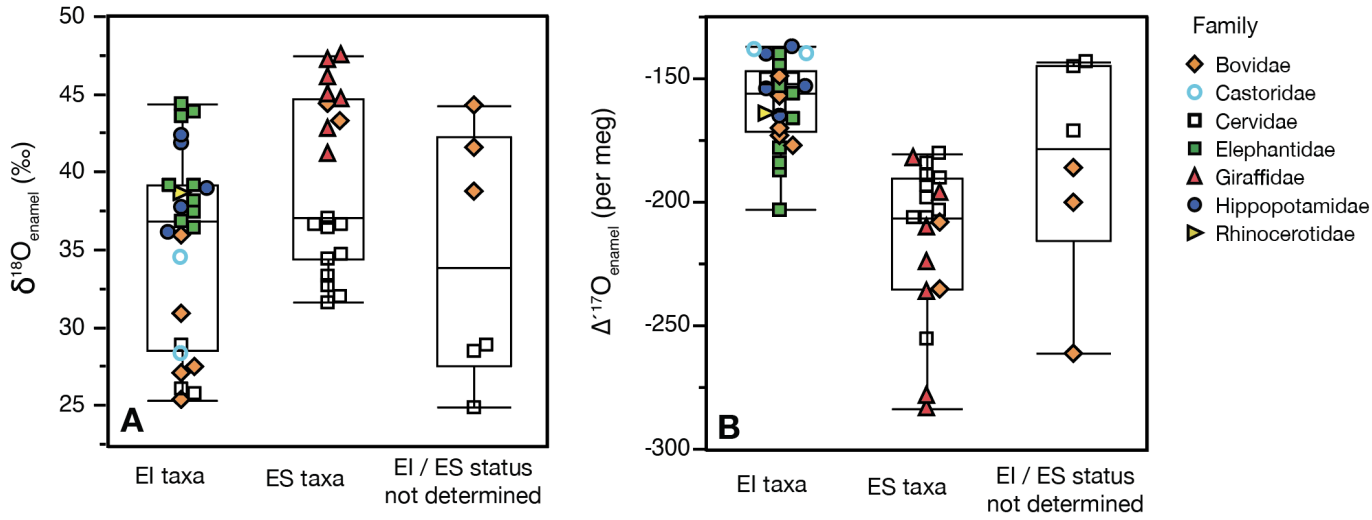

364

365

366 **Figure 4**: Box plots of A) $\delta^{18}O_{enamel}$ and B) $\Delta'^{17}O_{enamel}$ values of taxa grouped by the EI and ES

367 classification and plotted by family. Box ends are the quartile values, inner horizontal line the

368 median, and whiskers the range.

369

370

371 *4.1.2. $\Delta'^{17}O_{enamel}$ values in light of the $\Delta'^{17}O$ body water model*

372 Accurate isotope mass-balance body water models are critical for understanding the

373 controls on oxygen isotopic variation in tooth enamel. Of the body water models developed for

374 $\delta^{18}O$, some are scaled to body mass and metabolic rate (e.g., Bryant and Froelich, 1995),

375 whereas others consider animal behavior and physiology which can influence $\delta^{18}O$

376 independently of animal mass (e.g., Kohn, 1996). The latter is effective at predicting $\delta^{18}O_{enamel}$

377 across aridity gradients (e.g., Blumenthal et al., 2017) because it accounts for variation in fluxes

378 of water that undergo evaporation, including both water that is consumed (e.g., leaf waters,

379 surface waters) and released by an animal (e.g., vapor loss during breathing, panting).

With increased interest in triple oxygen isotopes, isotope mass-balance body water models have been adapted to consider $\Delta'^{17}O$, using approaches that either scale to animal mass (Pack et al., 2013; Whiteman et al., 2019) or link to animal physiology and behavior (Passey and Levin, 2021; Hu et al., *in revision*). While some studies demonstrate positive trends between $\Delta'^{17}O$ values of body water ($\Delta'^{17}O_{bw}$) and body mass (Pack et al., 2013; Whiteman et al., 2019), there is considerable scatter in $\Delta'^{17}O_{bw}$ values (> 200 per meg) among animals that do not vary in body mass but that do vary in WEI (Passey and Levin, 2021). This latter observation indicates the importance of physiology, behavior, and environment in determining $\Delta'^{17}O$ values in animals, as has been observed for $\delta^{18}O$ (e.g., Luz et al., 1990; Levin et al., 2006; Blumenthal et al., 2017).

Here we compare the $\Delta'^{17}O_{enamel}$ results from this study to outputs from an isotope mass-balance model to understand why $\Delta'^{17}O_{enamel}$ values vary among different taxa and across environmental gradients. We use a modeling approach that allows for the adjustment of fluxes of oxygen in and out of animals based on a version of the Kohn (1996) model that is modified for triple oxygen isotopes (Passey and Levin, 2021; Hu et al., *in revision*). We modeled animal physiology and behavior in four different scenarios: 1) a standard evaporation-sensitive condition where an animal is efficient with its water use (low WEI), has dry feces and consumes a large relative fraction of leaf water (e.g., giraffe, deer); 2) a water-dependent animal with high WEI, wet feces, but with a low proportion of consumed leaf water (e.g., hippos, beaver); 3) another water-dependent condition where an animal has a high WEI and wet feces, but consumes a high proportion of leaf water (e.g., elephant); and 4) an evaporation-sensitive condition where an animal has low WEI and dry feces but consumes very little leaf water (e.g.,

reindeer, caribou). These four different diet-physiology models are represented by the four different lines in Figure 5A-B. Model conditions are presented in Supplementary Tables 6 and 7. In these models, we use rh to represent environmental variation as it is a physical parameter that controls oxygen isotope fractionation, in contrast to using the AI or water deficit terms which are used to characterize environment of a particular place during average conditions (Supplementary Table 8).

For comparison to our $\Delta'^{17}O_{enamel}$ results, we calculated the equivalent mineral (enamel) composition from body water models using the $^{18/16}\alpha_{enamel\text{-}bw} = 1.0332$ and $\lambda_{enamel\text{-}bw} = 0.5245$, using the approaches outlined in Passey and Levin (2021) (Fig. 5A). To do this, we assume the triple oxygen isotope fractionation between body water and enamel ($\lambda_{enamel\text{-}bw}$) is similar to that for water and calcite ($\lambda_{calc\text{-}water}$). In recognition that $\lambda_{enamel\text{-}bw}$ may be different than 0.5245, we explored how changing $\lambda_{enamel\text{-}bw}$ affects model output. Figure 5B displays how a decrease in $\lambda_{enamel\text{-}bw}$ to 0.5237 results in a downward shift in the $\Delta'^{17}O$ results from all four models so they span our observed results.

Regardless of the specific $\lambda_{enamel\text{-}bw}$ used, the four modeled scenarios span the range in $\Delta'^{17}O_{enamel}$ values observed (Fig. 5). The standard evaporation-sensitive scenario (Model 1) captures minimum $\Delta'^{17}O$ values that decrease in more arid conditions (low rh), whereas the maximum water dependency model (Model 2) captures the upper range of $\Delta'^{17}O_{enamel}$ values where there is little variation with aridity. The outputs from Models 3 and 4 represent variants of these scenarios, with different combinations of WEI and leaf-water consumption, that yield $\Delta'^{17}O_{enamel}$ values that plot between those from Models 1 and 2. Changing the WEI adjusts the relative value of $\Delta^{17}O_{enamel}$ (low WEI matches low $\Delta'^{17}O_{enamel}$), whereas adjusting the proportion of

leaf water consumed, changes the sensitivity of $\Delta'^{17}O_{enamel}$ to rh (consumption of more leaf water increases sensitivity to rh).

The combination of modeled scenarios shows that 1) more water-efficient (low WEI) animals, such as giraffe and deer, should have lower $\Delta'^{17}O_{enamel}$ values than less water-efficient animals (high WEI) like hippos and beavers (Fig. 5) and 2) $\Delta'^{17}O_{enamel}$ values should decrease with increasing aridity, especially for animals with low WEI. These outputs capture the trends in the observed $\Delta^{17}O_{enamel}$ data: ES taxa yield lower $\Delta'^{17}O_{enamel}$ values than EI taxa (Fig. 4B) and $\Delta^{17}O_{enamel}$ values decrease with increased aridity (Figs. 3, 5). The model-data comparison here confirms the strong influences of both diet and physiology and environment on $\Delta^{17}O_{enamel}$ values identified by Passey and Levin (2021) and Hu et al. (*in revision*). $\Delta^{17}O_{enamel}$ varies within a guild of mammals in a single environment, due to differences in behavior, physiology, water-use strategy, and also across environments.

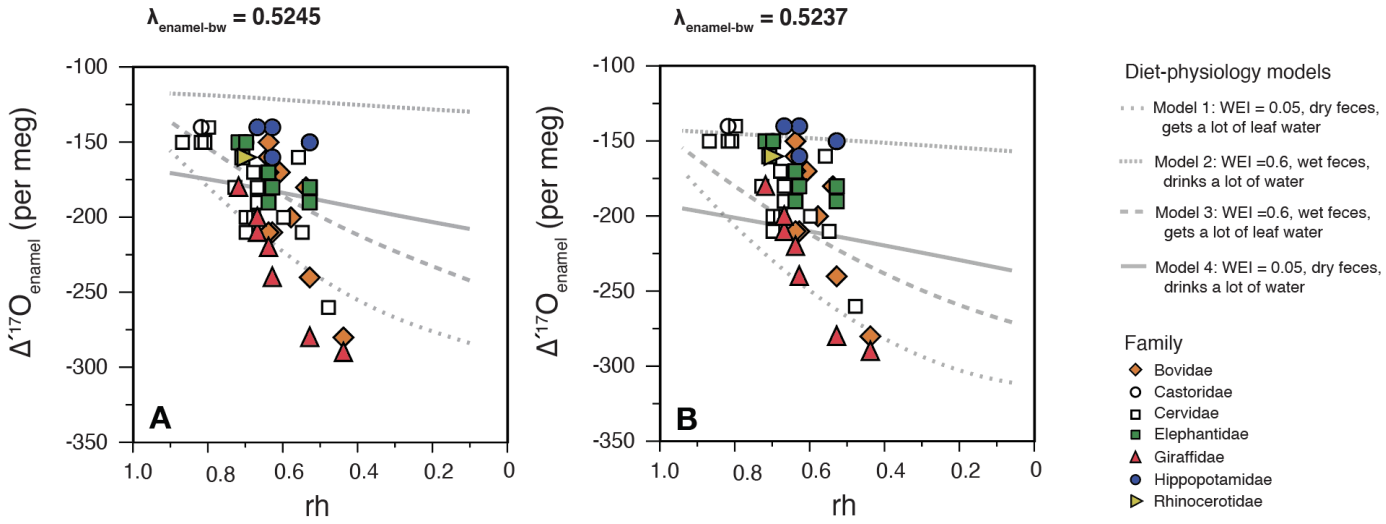

Figure 5: Observed $\Delta'^{17}O_{enamel}$ values from this study compared to how modeled outputs of $\Delta'^{17}O_{enamel}$ values vary with relative humidity (rh), based on a version of the Kohn (1996) model

that is modified for triple oxygen isotopes (Passey and Levin, 2021; Hu et al. *in revision*). Each line represents modeled outputs using different diet-physiology scenarios (Models 1-4), where WEI, feces water content, and drinking water amounts vs. leaf water consumption are varied. Modeled body water $\Delta'^{17}O$ values are converted to $\Delta'^{17}O_{enamel}$ assuming $^{18/16}\alpha_{enamel\text{-}bw}$ = 1.0332 using the approaches outlined in Passey and Levin (2021) and varying the value used for $\lambda_{enamel\text{-}bw}$ (0.5245 vs. 0.5237).

4.2. Applying $\Delta'^{17}O_{enamel}$ from large mammalian herbivores to reconstruct past aridity

Considering the generalized $\Delta'^{17}O_{enamel}$ – aridity relationship among extant animals, across a range of geographic and climate settings, we suggest that $\Delta'^{17}O_{enamel}$ of fossils can be used to assess past aridity. In the following text we discuss the use of $\Delta'^{17}O_{enamel}$ values of fossil mammalian herbivores as an indicator of past aridity and the advantages to using $\Delta'^{17}O_{enamel}$ values rather than approaches that rely on $\delta^{18}O_{enamel}$ alone.

4.2.1. $\Delta'^{17}O_{enamel}$ as an indicator of aridity

The $\Delta'^{17}O_{enamel}$ data from modern mammalian herbivores plot in a wedge-shaped pattern with AI that is consistent across geographic regions and among different taxa; the variance in $\Delta'^{17}O_{enamel}$ values is greatest in more arid environments. Translating this to the fossil record means that variations of $\Delta'^{17}O_{enamel}$ values from fossil assemblages may be used to infer relative differences in aridity between sites, such that sites with greater variance in $\Delta'^{17}O_{enamel}$ values represent more arid conditions than sites where $\Delta'^{17}O_{enamel}$ values are tightly clustered.

When using $\Delta'^{17}O_{enamel}$ values of fossils to compare aridity between sites and through time, sample sets should include taxa from the full range of water-use strategies available in a fossil assemblage. This increases the chances for $\Delta'^{17}O_{enamel}$ values in the sample set to capture the range in $\Delta'^{17}O_{enamel}$ values among a population from one place. In our study of extant mammals, we targeted teeth from animals with a range of water-use strategies from each site, but limited our analysis to only two samples for many sites to keep the analytical scope of the project manageable (e.g., hippopotamids/elephantids vs. giraffids) (Supplementary Table 1). Even with limited sampling, we observe greater variation in $\Delta'^{17}O_{enamel}$ values with increasing aridity. We would likely observe a greater variation in $\Delta'^{17}O_{enamel}$ values with bigger sample sizes, meaning that the variation in $\Delta'^{17}O_{enamel}$ values from any place would only provide an indication of minimum aridity for a site.

In the most basic sense, $\Delta'^{17}O_{enamel}$ values of fossil teeth can be used as a way to gage relative differences in aridity between fossil sites. However, the results of $\Delta'^{17}O_{enamel}$ from fossils can also be considered in terms of the UNESCO climate categories. Pooling our observations from three continents, the expected ranges for $\Delta'^{17}O_{enamel}$ values from guilds of mammalian herbivores are approximately 50 per meg in humid climates, 120 per meg in semi-arid climates, and 140 per meg in arid climates (Figs. 3B, 3E). We expect adjustments to these values as more individuals, taxa, and environments are sampled and added to this global dataset.

4.2.2. Advantages of using $\Delta'^{17}O$ as an aridity indicator compared to using $\delta^{18}O_{enamel}$ alone

The relationship between $\Delta^{17}O_{enamel}$ values and aridity is compelling as a paleoaridity indicator because it persists across a wide range of sites, with varying geography and $\delta^{18}O$

484 values of meteoric water, and among different combinations of mammalian taxa. In contrast,
485 we do not observe similarly clear relationships between $\delta^{18}O_{enamel}$ values and aridity because
486 $\delta^{18}O_{enamel}$ values are influenced by many other parameters in addition to aridity. As such,
487 $\delta^{18}O_{enamel}$ based reconstructions of aridity depend on the identification of taxa that fit into clear
488 ES and EI categories to control for the varying isotopic composition of local waters, but this
489 limits the extent of its application (e.g., Blumenthal et al., 2017).
490
491 *4.2.3. Application guidelines*
492 Below we outline an approach for sampling fossil mammalian herbivore teeth for the
493 purpose of estimating paleoaridity from $\Delta'^{17}O_{enamel}$ values. We present different scenarios based
494 on sample availability and provide suggestions for how $\Delta^{17}O_{enamel}$ data from fossils can be
495 compared with the modern dataset and then placed in a UNESCO climate category.
496 Sample sizes. In this study, we were not able to analyze more than one individual per
497 taxon for many sites, but for the places where we did sample more than one individual per
498 taxon, we find limited variation in $\Delta'^{17}O_{enamel}$ values amongst individuals (e.g., Turkana hippos: -
499 153±0.7 per meg, *n*=2; Garamba giraffes -203±10 per meg, *n*=2). Given this we conclude that
500 $\Delta'^{17}O_{enamel}$ data from a single animal provide valuable information, especially if from an ES taxon.
501 Whenever possible, sample sets should include more than one specimen of each taxon to
502 estimate intra-taxon variability of $\Delta'^{17}O_{enamel}$ values. However, given the fidelity of $\Delta'^{17}O_{enamel}$
503 values to environment, intra-taxon variability is expected to be relatively small.
504 Limited specimens. Considering that it is not always possible to sample numerous teeth
505 from a site (e.g., poor preservation, restricted sampling permission), we recommend targeting

samples that represent a range of water-use strategies to capture the greatest possible $\Delta'^{17}O_{enamel}$ variation. If on the other hand you can only sample a few taxa, then water-efficient taxa should be prioritized as their $\Delta'^{17}O_{enamel}$ values are likely to represent the minimum $\Delta'^{17}O_{enamel}$ values from a place, which could then be compared to $\Delta'^{17}O_{enamel}$ values of water-efficient taxa from other fossil sites to assess distinctions in aridity between sites. Our data show that site differences in $\Delta'^{17}O_{enamel}$ can help identify environmental distinctions when $\delta^{18}O_{enamel}$ cannot. For example, the giraffid $\Delta'^{17}O_{enamel}$ values arid sites are the most negative values in the entire dataset and are within 8 per meg of each other, with -278±10 and -283±3 per meg, for Kgalagadi and Turkana, respectively (Supplementary Table 1). This similarity is likely due to the arid (AI < 0.2) conditions of both places, despite differences in latitude (~4.6°N vs ~25.7°S), annual temperature (28°C vs 20°C), and $\delta^{18}O$ value for average annual meteoric water (~1‰ vs ~-5‰ VSMOW). In contrast, the $\delta^{18}O_{enamel}$ values of these two giraffids are indistinguishable from the $\delta^{18}O_{enamel}$ values of giraffids from mesic and humid sites (Fig. 3D).

Unknown ES and EI assignment. If there is limited *a priori* knowledge of the behaviors, physiologies, and water-use strategies from fossil herbivores at a site, and it is difficult to target a range of taxa that represent both ES and EI taxa, then a variety of taxa should be sampled to increase the potential of capturing the full range of $\Delta'^{17}O_{enamel}$ values at a site. By including taxa with a variety of water-use strategies, a dataset is more likely to capture the range in $\Delta'^{17}O_{enamel}$ values that represents a site's environment.

4.3. Other geological applications for $\Delta'^{17}O_{enamel}$ of large mammalian herbivores

4.3.1. Past pCO_2

528 We are not aware of other studies that propose the use of $\Delta'^{17}O_{enamel}$ values as indicators
529 of paleoaridity, but a handful of recent studies have suggested the use of $\Delta'^{17}O$ values from
530 teeth and eggshells to constrain past atmospheric pCO_2 (Pack et al., 2013; Gehler et al., 2016;
531 Passey et al., 2014; Passey and Levin, 2021). This is an exciting development given the
532 importance of understanding the history of Earth's pCO_2. This approach has been applied to
533 reconstruct pCO_2 across the Paleocene-Eocene Thermal Maximum (PETM); Gehler et al. (2016)
534 use a 60 per meg decrease in $\Delta'^{17}O_{enamel}$ values across the PETM to infer a ca. 400 to 1000 ppm
535 increase in atmospheric pCO_2. This approach works because inhaled atmospheric O_2, which has
536 a $\Delta'^{17}O$ value considerably lower than any form of water (Fig. 1), contributes between 5% to
537 40% of mammalian body water oxygen. As such, the $\Delta'^{17}O$ value of atmospheric O_2 is apparent
538 in tooth enamel $\Delta'^{17}O$ values; it pushes the $\Delta'^{17}O$ values of body water and enamel more
539 negative than the influences of food and drinking water oxygen alone (Pack et al., 2013). The
540 $\Delta'^{17}O$ value of atmospheric O_2 is influenced by mass independent fractionation of oxygen
541 isotopes in the stratosphere, where higher concentrations of atmospheric CO_2 leads to
542 decreased $\Delta'^{17}O$ values of atmospheric O_2 (Luz et al., 1999; Bao et al., 2008), and in turn, lower
543 $\Delta'^{17}O_{enamel}$ values (Pack et al., 2013).
544 Currently, $\Delta'^{17}O_{enamel}$-based estimates of pCO_2 are calculated from animals with small
545 body mass and high respiration rates (Gehler et al., 2016). These estimates do not consider how
546 $\Delta'^{17}O_{enamel}$ values vary among taxa (aside from differences in body mass) or in different
547 environments. But such variation is important; a 60 per meg distinction in $\Delta'^{17}O_{enamel}$ values that
548 is used to infer changes in pCO_2 can also be observed within an arid location among different
549 animals (e.g., Turkana) or between environments (e.g., 60 per meg represents the difference

between a subhumid and arid environment; Fig. 3). Given the similar magnitude of change in $\Delta'^{17}O_{enamel}$ values that occurs with a change in environment, animal taxon, or pCO_2 it will be essential to characterize the influence of environment on $\Delta'^{17}O_{enamel}$ values of mammalian herbivores before using them to infer pCO_2. To do this, we suggest sampling teeth from a range of taxa and from multiple fossil sites within a single time interval. Sites from a single time period across the globe should have similar atmospheric pCO_2. If pCO_2 is significantly different from today, then there will be a wholesale shift in $\Delta'^{17}O_{enamel}$ values away from the modern distribution of $\Delta'^{17}O_{enamel}$ values across multiple fossil sites, environments, and populations of taxa. We recognize that assessing past pCO_2 using $\Delta'^{17}O_{enamel}$ will require further study, but any use of $\Delta'^{17}O_{enamel}$ as a proxy for CO_2 needs to consider environmental and taxonomic variation in $\Delta'^{17}O_{enamel}$ values.

4.3.2. Diagenesis

Assessing and accounting for the role of diagenesis on $\delta^{18}O$ values of biocarbonate (i.e., tooth, bone, eggshell) has been a longstanding challenge in their use for paleoclimate reconstructions (e.g., Iacumin et al., 1996; Schoeninger et al., 2003). Any post-depositional reprecipitation of carbonate reflects the temperatures and isotopic composition of waters of this secondary event, not the biomineralization in an animal. The influence of reprecipitated carbonate on $\delta^{18}O_{enamel}$ values can be evaluated by comparing $\delta^{18}O_{enamel}$ values among different taxa, the $\delta^{18}O$ of phosphate in the same tooth enamel, or to the $\delta^{18}O$ of sedimentary carbonates. The elemental composition of bioapatite using x-ray diffraction and infrared spectroscopy can also be analyzed (e.g., Person et al., 1995; Iacumin et al., 1996).

572 The triple oxygen isotope composition of carbonates and bioapatites provides another
573 way to evaluate the effects of diagenesis (Gehler et al., 2011). Animal tissue $\Delta'^{17}O$ values are
574 more negative and more variable than the $\Delta'^{17}O$ values of carbonates derived from meteoric
575 waters due to the influence of low-$\Delta'^{17}O$ inhaled atmospheric O_2 and the strong roles of
576 environment and animal water-use that results in varying $\Delta'^{17}O$ values (Fig. 6).
577 The clear distinction between $\Delta'^{17}O$ values of biological carbonates and meteoric
578 carbonates means that $\Delta'^{17}O$ measurements can be used to evaluate diagenesis of the original
579 oxygen isotopic composition of biocarbonate without relying on additional analyses and
580 materials. Gehler et al. (2011) suggests the $\Delta'^{17}O$ values of tissue from small mammals (< 1 kg)
581 can help evaluate diagenesis. This concept is also relevant for larger mammals (> 6 kg) and
582 birds, as $\Delta'^{17}O$ values of tooth enamel and eggshells are more negative and more variable than
583 those of meteoric-derived carbonates (Fig. 6). However, there are some exceptions; carbonates
584 formed from waters that are extensively evaporated, such as closed basin, saline Mono Lake,
585 can have $\Delta'^{17}O$ values as low as -214 per meg (see Passey and Ji, 2019) and fall squarely in the
586 range of $\Delta'^{17}O$ values of bird and mammal biocarbonate.
587 To use $\Delta'^{17}O$ analyses to determine diagenesis of fossil enamel, a sample set should
588 include both fossils from taxa with a range of water-use strategies and carbonates that are
589 available from the sediments associated with the fossils (e.g., soil carbonate, lacustrine
590 carbonate, cements). If the $\Delta'^{17}O_{enamel}$ values are unaltered, then they will be more negative and
591 varied than that of the associated carbonates. If the $\Delta'^{17}O$ values of carbonates and enamel are
592 similar, then the distribution of $\Delta'^{17}O_{enamel}$ values will be compressed and the original oxygen

isotopic composition of the fossil teeth has been altered. This concept can be extended to other fossil biocarbonates like bones and eggshells.

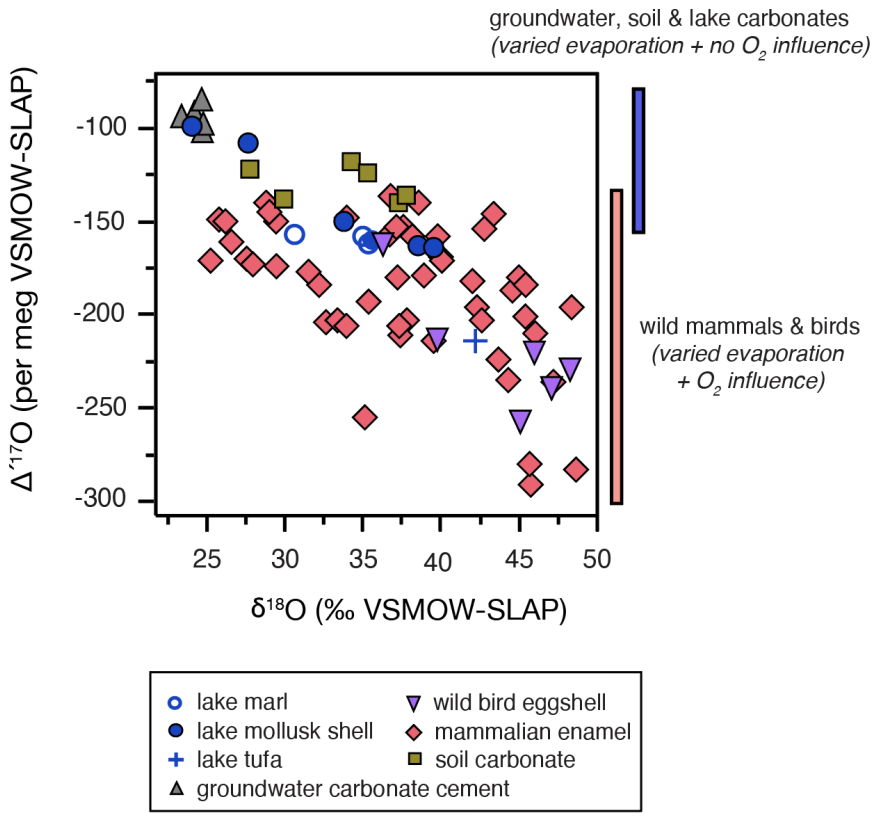

Figure 6: The $\Delta'^{17}O$ and $\delta^{18}O$ values of large mammalian tooth enamel, bird eggshells, mollusks, and groundwater cement, lake, and soil carbonates. Data are from Passey et al. (2014), Passey and Ji (2019), Hu et al. (*in revision*), and this study.

5. Conclusions

The $\Delta'^{17}O_{enamel}$ values of extant, large mammalian herbivores sampled from three continents and seven mammalian families vary by 146 per meg (-283 to -137 per meg). The

relationship between $\Delta'^{17}O_{enamel}$ values and aridity form a wedge-shaped pattern, with greater variation in $\Delta'^{17}O_{enamel}$ values in arid environments. This relationship is independent of latitude and $\delta^{18}O$ value of local meteoric waters. However, the relationship between $\Delta'^{17}O_{enamel}$ values does depend on animal water-use strategy; generally, $\Delta'^{17}O_{enamel}$ values from water-dependent animals vary little with aridity, whereas water-efficient animals yield lower $\Delta'^{17}O_{enamel}$ values that decrease with aridity.

Our dataset provides a framework for using $\Delta'^{17}O_{enamel}$ values to evaluate aridity of past environments. The $\Delta'^{17}O_{enamel}$ values from multiple taxa in a fossil assemblage can be used to estimate the paleoaridity of a fossil site and roughly place it into one of the UNESCO climate categories. The use of $\Delta'^{17}O_{enamel}$ values broadens the utility of the oxygen isotope composition of terrestrial materials for paleoenvironmental reconstructions, because their distribution is so tied to aridity, unlike $\delta^{18}O$ values of enamel (and other materials) which are influenced by a combination of multiple factors (e.g., aridity, temperature, $\delta^{18}O$ values of meteoric water).

In addition to their utility for paleoenvironmental reconstructions, $\Delta'^{17}O$ values of fossil teeth can be used to estimate past pCO_2 and evaluate diagenetic effects on the oxygen isotope composition of samples. Our expanded dataset from extant herbivores shows the importance of sampling teeth from a range of taxa for both of these approaches to work effectively. Studies that use $\Delta'^{17}O_{enamel}$ values as a pCO_2 indicator must first account for the range of $\Delta'^{17}O_{enamel}$ variation due to the environment and animal water-use strategy. Likewise, any study using $\Delta'^{17}O_{enamel}$ values to identify diagenesis should include samples from taxa with different water-use strategies because they should yield $\Delta'^{17}O_{enamel}$ values that are relatively wide-ranging if unaltered and relatively invariant if altered. These results show the expanded potential for the

627 utility of triple oxygen isotope distributions in biocarbonates. The next steps for this work
628 include expanding the sample from extant animals to include more individuals from a broader
629 range of geographic settings and then applying this framework to constrain aridity, pCO_2, and
630 diagenesis in Earth's past.
631
632
633 **Acknowledgements**
634 We thank David Patterson, Scott Blumenthal, and staff from the Edness Kimball Wilkins State
635 National Park, WY for providing samples for analysis. We also thank Scott Blumenthal for
636 sharing his Matlab code for extracting water isotope data from WorldClim 1.4 and for
637 assistance in extracting climate information for each site. We thank the Department of Earth
638 and Planetary Sciences Department at Johns Hopkins University where samples were prepared
639 and analyzed. A Johns Hopkins Early Career Catalyst Grant awarded to Naomi Levin funded this
640 work.

Figure list

Figure 1: $\Delta'^{17}O$ and $\delta^{18}O$ values of waters and reconstructed waters from carbonates.

Figure 2: Schematic outlining the variation of $\delta^{18}O_{enamel}$ and $\Delta'^{17}O_{enamel}$ values with aridity for different mammalian herbivore taxa.

Figure 3: Variation in $\delta^{18}O_{enamel}$ and $\Delta'^{17}O_{enamel}$ values by latitude, location, taxon, and climate.

Figure 4: Box plots of (A) $\delta^{18}O_{enamel}$ and (B) $\Delta'^{17}O_{enamel}$ of taxa grouped by evaporation sensitivity.

Figure 5: The $\Delta'^{17}O$ and $\delta^{18}O$ values of large mammalian tooth enamel, bird eggshells, and lake and soil carbonates.

Figure S1: Distribution of (a) $\delta^{18}O_{enamel}$ and (b) $\Delta'^{17}O_{enamel}$ data. From left to right: Histogram of data with a normal continuous fit. Quantile box plot with horizontal lines as median and quantile groups, points as outliers, and brackets as the region of densest data. Normal quantile plot with line of fit, the empirical cumulative probability and normal quantile scales, and Lilliefors confidence bounds (dotted line).

Table List

681 Table S8. Modeled body water and enamel oxygen isotopes with relative humidity and Aridity

682 Index.

683

684 **Table 1.** Geographic, climatic and environmental information for sample locations.

685

Country	Location	Latitude	Longitude	CRU output mean rh (%)	OIPC 3.1 $\delta^{18}O$ MAP (‰ SMOW)	RCWIP $\delta^{18}O$ MAP (‰ SMOW)	MAP (mm/yr)	MAT (°C)	PET (mm/yr)	WD (mm/yr)	Aridity Index	Aridity Index UNESCO category
Africa												
Kenya	Turkana	4.3641	35.663	52.9	1.1	0.2	347	28	1897	1550	0.18	arid
Kenya	Meru National Park	0.0806	38.1979	63.2	1.7	-0.5	512	24.5	2064	1552	0.24	semi-arid
Kenya	Shimba Hills National Park	-4.2572	39.3878	70.9	-3.5	-1.4	1137	23.9	1493	356	0.75	semi-arid
Kenya	Laikipia/Mpala National Park	0.348	36.9924	63.9	-0.8	-4.8	713	18.2	1782	1069	0.39	semi-arid
Kenya	Tsavo National Park	-2.3661	38.4098	63.3	0.8	-1.3	670	25	1836	1166	0.37	semi-arid
Kenya	Aberdares National Park	-0.4359	36.717	70.2	-3.6	-9.0	1780	10.1	1196	-584	1.52	humid
Ethiopia	Awash National Park	9.0833	40	62.6	2.2	-1.0	525	25.9	2091	1566	0.25	semi-arid
Uganda	Kidepo National Park	3.8604	33.8549	57.9	-1.1	-1.7	614	22.9	1720	1106	0.34	semi-arid
DR Congo	Garamba National Park	4.1665	29.5003	67.1	0.2	-1.5	1548	24.4	1813	265	0.86	humid
DR Congo	Ituri Forest National Park	1.4043	28.5769	71.6	-0.2	-2.1	1739	24.4	1771	32	0.98	humid
South Africa	Kgalagadi National Park	-25.7488	20.4436	43.8	-4.7	-3.7	230	20	1878	1648	0.12	arid
South Africa	Addo National Park	-33.5023	25.7721	64.2	-3.7	-3.2	424	17.9	1398s	974	0.32	semi-arid
Europe												
Finland	Noormarkku	61.5908	21.8671	81.6	-12.0	-11.5	608	4	548	-60	1.11	humid
Finland/Sweden	Karessuando	68.438	22.4511	86.5	-14.9	-14.2	448	-2.2	393	-55	1.14	humid
Finland	Rovaniemi	66.5181	25.669	80.0	-13.1	-13.5	513	0.4	458	-55	1.13	humid
Finland	Pernaja	60.4386	26.0528	81.1	-11.8	-11.8	618	4.7	547	-71	1.13	humid
Karelia, Russia	Aunus Nurmoila	61.07513	32.924	81.8	-12.0	-12.3	672	2.9	541	-131	1.24	humid
North America												
United States	Badlands National Park, SD	43.8554	-102.34	60.5	-9.9	-11.5	415	8.6	1109	694	0.37	semi-arid
United States	Theodore Roosevelt National Park, ND	46.979	-103.539	63.9	-11.4	-13.0	383	6.3	982	599	0.40	semi-arid
United States	Wichita Mountains Federal Wildlife Refuge, OK	34.7223	-98.7345	63.7	-5.8	-6.7	735	15.4	1358	623	0.54	subhumid
United States	Antelope Island, UT	40.9581	-112.215	54.3	-14.1	-10.1	462	10.1	1026	564	0.57	subhumid
United States	Parowan, UT	37.8352	-112.829	48.1	-12.7	-11.7	320	8.9	1229	909	0.26	semi-arid
United States	Arctic National Wildlife Refuge, AK	68.6496	-142.898	67.9	-26.0	-24.2	154	-13.9	263	109	0.58	subhumid
United States	Middle Fork, Selman River, ID	44.9305	-114.965	59.9	-16.6	-15.1	581	-0.1	789	208	0.74	subhumid
United States	Piedmont National Wildlife Refuge, GA	33.0864	-83.7275	70.2	-5.5	-5.5	1213	17.3	1415	202	0.86	humid
United States	Berkley Springs, WV	39.6249	-78.2387	69.6	-8.2	-8.0	949	10.7	1093	144	0.87	humid
United States	Baltimore, MD	39.3068	-76.6316	66.6	-6.7	-6.5	1110	12.9	1142	32	0.96	humid
United States	Westchester County, NY	41.122	-73.7949	67.7	-7.6	-8.3	1227	10.6	980	-247	1.26	humid
United States	Dairymens Country Club, WI	46.1453	-89.6576	72.6	-10.8	-11.9	834	3.8	819	-15	1.02	humid
United States	Yellowstone National Park, WY	44.428	-110.588	55.7	-16.8	-17.2	646	-1	760	114	0.82	humid
United States	Edness Kimball Wilkins State National Park, WY	42.8536	-106.182	55.3	-13.0	-12.9	311	7.9	1105	794	0.28	semi-arid

686
687

688 **Table 2.** Animal behavior summary for reported taxa

Common name	Family	Genus and species	Diet	General water use strategy	ES or EI status[a]
Red/Cape hartebeest	Bovidae	*Alcelaphus buselaphus caama*	Grazer	[e, i]Not very water dependent	-
Bison	Bovidae	*Bison bison bison*	Grazer	[h]Water dependent	EI
Blue wildebeest	Bovidae	*Connochaetes taurinus taurinus*	Grazer	[i]Not very water dependent	-
Oryx	Bovidae	*Oryx gazella beisa*	Grazer	[b, e, i]Not water dependent	ES
African buffalo	Bovidae	*Syncerus caffer*	Grazer	[e, i]Water dependent	-
Beaver	Castoridae	*Castor fiber*	Semi-aquatic	[d]Water dependent	EI
Moose	Cervidae	*Alces alces*	Mixed feeder/Semi-aquatic	[d]Water dependent	EI
White-tailed deer	Cervidae	*Odocoileus virginianus virginianus*	Mixed feeder	[c]Not water dependent	ES
Reindeer and Caribou	Cervidae	*Rangifer tarandus*	Browser/Mixed feeder	[d]Not very water dependent	-
Elephant	Elephantidae	*Loxodonta africana africana*	Browser	[i]Water dependent	EI
Giraffe	Giraffidae	*Giraffa camelopardalis*	Browser	[g, i]Not water dependent	ES
Okapi	Giraffidae	*Okapia johnstoni*	Browser	[f, g, i]Not water dependent	ES
Hippo	Hippopotamidae	*Hippopotamus amphibius amphibius*	Semi-aquatic	[g, i]Water dependent	EI
Black rhino	Rhinocerotidae	*Diceros bicornis*	Browser/Grazer	[i]Water dependent	EI

[a] Data are classified as ES or EI based on the relationship between $\delta^{18}O$ values and aridity and relative humidity based on previously published work. For taxa that have not been classified as ES and EI, we evaluated their diet, water use, and WEI when available to suggest ES or EI classification.

References ([b]Kohn et al., 1996; [c]Luz et al., 1990; [d]Nowak, 1991; [e,f]Cerling et al., 2003; 2004; [g]Levin et al., 2006; [h]Hoppe et al., 2006; [i]Blumenthal et al. 2017)

689

690

691 **References**

692 Alexandre, A., Landais, A., Vallet-Coulomb, C., Piel, C., Devidal, S., Pauchet, S., Sonzogni, C.,
693 Couapel, M., Pasturel, M., Cornuault, P., Xin, J., Mazur, J.-C., Prié, F., Bentaleb, I., Webb, E.,
694 Chalié, F., Roy, J., 2018. The triple oxygen isotope composition of phytoliths as a proxy of
695 continental atmospheric humidity: insights from climate chamber and climate transect
696 calibrations. Biogeosciences. 15, 3223-3241.

697

698 Bao, H., Lyons, J.R., Zhou, C., 2008. Triple oxygen isotope evidence for elevated CO_2 levels after
699 a Neoproterozoic glaciation. Nature. 453, 504-506.

700

701 Barkan, E., Luz, B., 2005. High precision measurements of $^{17}O/^{16}O$ and $^{18}O/^{16}O$ ratios in H_2O.
702 Rapid Communications of Mass Spectrometry. 19, 3737-3742.

703

704 Barkan, E., Luz, B., 2007. Diffusivity fractionations of $H_2{}^{16}O/H_2{}^{17}O$ and $H_2{}^{16}O/H_2{}^{18}O$ in air and their
705 implications for isotope hydrology. Rapid Communications of Mass Spectrometry. 21,
706 2999-3005.

707

708 E. Barkan, E., Luz, B., 2011. The relationships among the three stable isotopes of oxygen in air,
709 seawater and marine photosynthesis. Rapid Commun. Mass Spectrom. 25, 2367-2369.

710

711 Blumenthal, S.A., Levin, N.E., Cerling, T.E., Brown, F.H., Brugal, J.-P., Chritz, K.L., Harris, J.M.,
712 Jehle, G.E., 2017. Aridity and early hominin environments. Proceedings of the National

713 Academy of Sciences. 114, 7331-7336.

714 Bowen, G.J., Revenaugh, J., 2003. Interpolating the isotopic composition of modern meteoric
715 precipitation. Water Resour. Res. 39, 1299.

716 Bryant J. D. and Froelich P. N. (1995) A model of oxygen isotope fractionation in body water of
717 large mammals. Geochim Cosmochim Acta 59, 4523–4537.

718

719 Dansgaard, W., 1964. Stable Isotopes in Precipitation. Tellus. 16, 436-468.

720

721 Fricke, H.C., O'Neil, J.R., Lynnerup, N., 1995. Oxygen isotope composition of human tooth
722 enamel from Medieval Greenland: linking climate and society. Geology. 23, 869-872.

723

724 Gehler, A., Gingerich, P.D., Pack, A., 2016. Temperature and atmospheric CO_2 concentration
725 estimates through the PETM using triple oxygen isotope analysis of mammalian bioapatite.
726 Proceedings of the National Academy of Sciences. 113, 7739-7744.

727

728 Gehler, A., Tütken, T., Pack, A., 2011. Triple oxygen isotope analysis of bioapatite as tracer for
729 diagenetic alteration of bones and teeth. Paleogeography, Paleoclimatology, Paleoecology. 310,
730 84-91.

731

732 Herwartz, D., Surma, J., Voigt, C., Assonov, S., Staubwasser, M., 2017. Triple oxygen isotope
733 systematics of structurally bonded water in gypsum. Geochimica Cosmochimica Acta 209. 254-

266.

Hijmans, R.J., Cameron, S.E., Parra, J.L., Jones, P.G., Jarvis, A., 2005. Very high resolution interpolated climate surfaces for global land areas. Int. J. Climatol. 25, 1965-1978.

Hu, H., Passey, B.H., Lehmann, S.B., Levin, N.E., Johnson, B.J., (*in revision*). Modeling and interpreting triple oxygen isotope variations in vertebrates, with implications for paleoclimate and paleoecology. Chemical Geology.

Iacumin, P., Bocherens, H., Mariotti, A., Longinelli, A., 1996. Oxygen isotope analyses of co-existing carbonate and phosphate inn biogenic apatite: a way to monitor diagenetic alteration of bone phosphate? Earth and Planetary Science Letters. 142, 1-6.

Kohn, M.J., 1996. Predicting animal $\delta^{18}O$: accounting for diet and physiological adaptation. Geochimica et Cosmochimica Acta. 60, 4811-4829.

Landais, A., Barkan, E., Yakir, D., Luz, B., 2006. The triple isotopic composition of oxygen in leaf water. Geochimica et Cosmochimica Acta. 70, 4105-4115.

Landais, A., Risi, C., Bony, S., Vimeux, F., Descroix, L., Falourd, S., Bouygues, A., 2010. Combined measurement of ^{17}O-excess and d-excess in African monsoon precipitation: Implication for evaluating convective parameterizations. Earth and Planetary Science Letters. 298, 104-112.

Lécuyer, C., Balter, V., Martineau, F., Fourel, F., Bernard, A., Amiot, R., Gardien, V., Otero, O., Legendre, S., Panczer, G., Simon, L., Martini, R., 2010. Oxygen isotope fractionation between apatite-bound carbonate and water determined from controlled experiments with synthetic apatites precipitated at 10-37˚C. Geochimica et Cosmochimica Acta. 74, 2072-2081.

Levin, N.E., Cerling, T.E., Passey, B.H., Harris, J.M., Ehleringer, J. R., 2006. A stable isotope aridity index for terrestrial environments. Proceedings of the National Academy of Sciences. 103, 11201-11205.

Li, S., Levin, N.E., Soderberg, K., Dennis, K.J., Caylor, K.K., 2017. Triple oxygen isotope composition of leaf waters in Mpala, central Kenya. Earth and Planetary Science Letters. 468, 38-50.

Luz, B., Cormie, A.B., Schwarcz, H.P., 1990. Oxygen isotope variations in phosphate of deer bones. Geochimica et Cosmochimica Acta. 54, 1723-1728.

Luz, B., Barkan, E., Bender, M.L., Thiemens, M.H., Boering, K.A., 1999. Triple-isotope composition of atmospheric oxygen as a tracer of biosphere productivity. Nature. 400, 547-550.

Luz, B., Barkan, E., 2005. The isotopic ratios $^{17}O/^{16}O$ and $^{18}O/^{16}O$ in molecular oxygen and their significance in biogeochemistry. Geochimica et Cosmochimica Acta. 69, 1099-1110.

778

779 Luz, B., Barkan, E., 2010. Variations of $^{17}O/^{16}O$ and $^{18}O/^{16}O$ in meteoric waters. Geochimica et

780 Cosmochimica Acta. 74, 6276-6286.

781

782 Matsuhisa, Y., Goldsmith, J.R., Clayton, R.N., 1978. Mechanisms of hydrothermal crystallization

783 of quartz at 250˚C and 15kbar. Geochimica et Cosmochimica Acta. 42, 173-182.

784

785 Miller, M.F., 2002. Isotopic fractionation and the quantification of ^{17}O anomalies in the oxygen

786 three-isotope system: an appraisal and geochemical significance. Geochimica et Cosmochimica

787 Acta. 66, 1881-1889.

788

789 Nagy, K.A., Peterson, 1988, Scaling of water flux rate in animals. University of California

790 Publications in Zoology, 120, 1–172.

791

792 Nowak, R., 1999, Walker's Mammals of the World. Sixth Edition. Baltimore. The Johns Hopkins

793 University Press.

794

795 Pack, A., 2021. Isotopic traces of atmospheric O2 in rocks, minerals, and melts. Reviews in

796 Mineralogy and Geochemistry. 86, 217-240.

797

798 Pack, A., Gehler, A., Süssenberger, A., 2013. Exploring the usability of isotopically anomalous

799 oxygen in bones and teeth as paleo-CO_2-barometer. Geochimica et Cosmochimica Acta. 102,

306-317.

Passey BH, Levin NE. 2021. Triple oxygen isotopes in meteoric waters, carbonates, and biological apatites: implications for continental paleoclimate reconstruction. Reviews in Mineralogy & Geochemistry. 86, 429-462.

Passey, B.H., Hu, H., Ji, H., Montanari, S., Li, S., Henkes, G.A., Levin, N.E., 2014. Triple oxygen isotopes in biogenic and sedimentary carbonates. Geochimica et Cosmochimica Acta. 141, 1-25.

Passey, B.H., Ji. H., 2019. Triple oxygen isotope signatures of evaporation in lake waters and carbonates: A case study from the Western United States. Earth and Planetary Science Letters. 518, 1-12.

Person, A., Bocherens, H., Saliège, J.F., Paris, F., Zeitoun, V., Gérard, M., Early Diagenetic Evolution of Bone Phosphate: An X-ray Diffractometry Analysis. Journal of Archaeological Science. 22, 211-221.

Rowley, D.B., Currie, B.S., 2006. Palaeo-altimetry of the late Eocene to Miocene Lunpola basin, central Tibet. Nature. 439, 677-681.

Rozanski, K., Aragua´s-Aragua´s, L., Gonfiantini, R., 1993. Isotopic patterns in modern global precipitation. In: Swart, P.K., Lohmann, K.C., McKenzie, J., Savin, S. (Eds.), Climate Change in

Continental Isotopic Records. American Geophysical Union Geophysical Monograph. American Geophysical Union. Washington, DC. 78, 1-36.

Schoenemann, S.W., Schauer, A.J., Steig, E.J., 2013. Measurement of SLAP2 and GISP $\delta^{17}O$ and proposed VSMOW-SLAP normalization for $\delta^{17}O$ and $\delta^{18}O$. Rapid Communications in Mass Spectrometry. 27, 582-590.

Schoeninger, M.J., Hallin, K., Reeser, H., Valley, J.W., Fournnelle, J., 2003. Isotopic alteration of mammalian tooth enamel. International Journal of Osteoarchaeology. 13, 11-19.

Sharp, Z.D., Wostbrock, J.A.G., 2021. Standardization for the triple oxygen isotope system: Waters, silicates, carbonates, air, and sulfates. Reviews in Mineralogy & Geochemistry. 86, 179-196.

Surma, J., Assonov, S., Bolourchi, M.J., Staubwasser, M., 2015. Triple oxygen isotope signatures in evaporated water bodies from the Sistan Oasis, Iran. Geophysical Research Letters. 42, 8456-8462.

Surma, J., Assonov, S., Herwartz, D., Voigt, C., Staubwasser, M., 2018. The evolution of ^{17}O-excess in surface water of the arid environment during recharge and evaporation. Scientific Reports. 8, 4972.

844 Trabucco, A., Zomer, R.J., 2009. Global Aridity Index (Global-aridity) and Global Potential Evapo-
845 transpiration (Global-PET) Geospatial Database. CGIAR Consortium for Spatial Information.
846 Published online, available from: the CGIAR-CSI GeoPortal. http://www.csi.cgiar.org/.
847
848 Uechi, Y., Uemura, R., 2019. Dominant influence of the humidity in the moisture source region
849 on the ^{17}O-excess in precipitation on a subtropical island. Earth and Planetary Science Letters.
850 513, 20-28.
851
852 UNESCO, 1979. Map of the world distributions of arid regions, explanatory note, MAB Technical
853 Notes, Paris.
854
855 Whiteman, J.P., Sharp, Z.D., Gerson, A.R., Newsome, S.D., 2019. Relating $\Delta^{17}O$ values of animal
856 body water to exogenous water inputs and metabolism. BioScience. 69, 658-688.
857
858 Wostbrock, J.A.G., Cano, E.J., Sharp, Z.D., 2020, An internally consistent triple oxygen isotope
859 calibration of standards for silicates, carbonates and air relative to VSMOW2 and SLAP2.
860 Chemical Geology 533, 119432.
861
862 Young, E.D., Galy, A., Nagahara, H., 2002. Kinetic and equilibrium mass-dependent isotope
863 fractionation laws in nature and their geochemical and cosmochemical significance. Geochimica
864 et Cosmochimica Acta. 66, 1095-1104.
865

866 Zachos, J., Pagani, M., Sloan, L., Thomas, E., Billups, K., 2001. Trends, rhythms, and

867 aberrations in global climate 65 Ma to present. Science. 292, 686-693.